

Syntheses, crystal structures and magnetic properties of two cyano-bridged two-dimensional assemblies $[\text{Fe}(\text{salpn})]_2[\text{Fe}(\text{CN})_5\text{NO}]$ and $[\text{Fe}(\text{salpn})]_2[\text{Ni}(\text{CN})_4]$

Xiao-Ping Shen and Zheng Xu*

Coordination Chemistry Institute, State Key Laboratory of Coordination Chemistry, Nanjing University, Nanjing 210093, PR China

Ai-Hua Yuan

Department of Material and Environmental Engineering, East China Shipbuilding Institute, Zhenjiang 212003, PR China

Zi-Xiang Huang

State Key Laboratory of Structural Chemistry, Fujian Institute of Research on the Structure of Matter, Chinese Academy of Sciences, Fuzhou, Fujian 350002, PR China

Received 13 May 2003; accepted 07 July 2003

Abstract

Two cyano-bridged assemblies, $[\text{Fe}^{\text{III}}(\text{salpn})]_2[\text{Fe}^{\text{II}}(\text{CN})_5\text{NO}]$ (1) and $[\text{Fe}^{\text{III}}(\text{salpn})]_2[\text{Ni}^{\text{II}}(\text{CN})_4]$ (2) [salpn = *N, N'*-1,2-propylenebis(salicylideneiminato)dianion], have been prepared and structurally and magnetically characterized. In each complex, $[\text{Fe}(\text{CN})_5\text{NO}]^{2-}$ or $[\text{Ni}(\text{CN})_4]^{2-}$ coordinates with four $[\text{Fe}(\text{salpn})]^+$ cations using four co-planar CN^- ligands, whereas each $[\text{Fe}(\text{salpn})]^+$ links two $[\text{Fe}(\text{CN})_5\text{NO}]^{2-}$ or $[\text{Ni}(\text{CN})_4]^{2-}$ ions in the *trans* form, which results in a two-dimensional (2D) network consisting of pillow-like octanuclear $[-\text{M}^{\text{II}}-\text{CN}-\text{Fe}^{\text{III}}-\text{NC}-]_4$ units ($\text{M} = \text{Fe}$ or Ni). In complex (1), the NO group of $[\text{Fe}(\text{CN})_5\text{NO}]^{2-}$ remains monodentate and the bond angle of $\text{Fe}^{\text{II}}-\text{N}-\text{O}$ is 180.0° . The variable temperature magnetic susceptibilities, measured in the 5–300 K range, show weak intralayer antiferromagnetic interactions in both complexes with the intramolecular iron(III)··iron(III) exchange integrals of -0.017 cm^{-1} for (1) and -0.020 cm^{-1} for (2), respectively.

Introduction

In recent years, an enormous amount of research work has been devoted to the study of cyano-bridged coordination polymers due to their potential use as functional solid materials, such as catalysts, optical devices as well as molecular-based magnets [1–5]. It is known that the cyano-bridged 3D bimetallic assemblies of the Prussian Blue type, derived from hexacyanometalate ions $[\text{M}(\text{CN})_6]^{m-}$ and simple transition metal ions, exhibit spontaneous magnetization at T_C as high as 376 K, and interesting optoelectronic and magneto-optical properties [6–10]. However, magneto-structural correlation of these high T_C or T_N compounds remains unclear because of the difficulty in obtaining single crystals. Furthermore, the face-centred cubic structures (based on powder XRD results) usually possess low or no magnetic anisotropy. To overcome these problems, a wide variety of hybrid Prussian Blue complexes assembled from cyanometalate building blocks $[\text{M}(\text{CN})_n]^{m-}$ ($\text{M} = \text{Fe}, \text{Cr}, \text{Co}, \text{Mn}, \text{Mo}$ and W etc.) and coordinatively unsaturated transition metal complexes have

been studied structurally and magnetically [11–16]. These complexes exhibit fascinating structures ranging from discrete entities to 3D extended networks, and interesting magnetic properties, such as magnetic ordering and high spin ground states. For example, the reaction between $[\text{M}'(\text{BS})]^+$ ($\text{M}' = \text{Mn}, \text{Fe}$; BS = Schiff base ligand) and $[\text{M}(\text{CN})_6]^{3-}$ ($\text{M} = \text{Fe}, \text{Cr}$) has already led to a variety of lattice structures depending on the nature of the Schiff base, the metal ion and the counteranion etc., e.g., the discrete heptanuclear complex $[\text{Cr}\{(\text{CN})\text{Mn}(\text{salen}\cdot\text{H}_2\text{O})\}_6][\text{Cr}(\text{CN})_6]\cdot 6\text{H}_2\text{O}$ [salen = *N, N'*-ethylenebis(salicylideneiminato)dianion] [17], the 1D chain complex $[\text{NEt}_4]_2\{\text{Mn}(\text{acacen})\}[\text{Fe}(\text{CN})_6]$ [acacen = *N, N'*-ethylenebis(acetylacetylidenaminato)dianion] [18], 2D network complexes $\{[\text{Mn}(\text{saltmen})\}_4\{\text{Fe}(\text{CN})_6\}\text{ClO}_4\cdot\text{H}_2\text{O}$ [saltmen = *N, N'*-(1,1,2,2-tetramethylethylene)bis(salicylideneiminato)dianion] [19] and $\{[\text{Fe}(\text{salen})\}_3\{\text{Fe}(\text{CN})_6\}(\text{MeOH})_2\cdot 3\text{H}_2\text{O}$ [20]. They exhibit the ferromagnetic or antiferromagnetic interaction between adjacent paramagnetic centers through the cyanide bridge. Recently, we have prepared two new cyano-bridged coordination polymers, $[\text{Fe}^{\text{III}}(\text{salpn})]_2[\text{Fe}^{\text{II}}(\text{CN})_5\text{NO}]$ (1) and $[\text{Fe}^{\text{III}}(\text{salpn})]_2[\text{Ni}^{\text{II}}(\text{CN})_4]$ (2) [salpn = *N, N'*-1,2-propylenebis

* Author for correspondence

(salicylideneiminato) dianion], using the Schiff base complex cation $[\text{Fe}(\text{salpn})]^+$ as a template. Here we report the syntheses, structures and magnetic properties of the two 2D assemblies with neutral layers.

Experimental

Physical measurements

Elemental analyses for C, H and N were performed with a Perkin-Elmer 240C analyzer. Fe and Ni analyses were made on a Jarrell-Ash 1100 + 2000 inductively coupled plasma quantummeter. I.r. spectra were recorded on a Nicolet FT-170SX spectrometer with KBr pellets in the 4000–400 cm^{-1} region. Magnetic susceptibilities on crystalline samples were measured with a Quantum Design MPMS-5 SQUID susceptometer under an applied magnetic field of 10 kOe in the 5–300 K range. Diamagnetic corrections were made using Pascal's constants. Effective magnetic moments were calculated using the equation $\mu_{\text{eff}} = 2.828(\chi_{\text{M}} \times T)^{1/2}$, where χ_{M} is the magnetic susceptibility per formula unit.

Syntheses

All chemicals and solvents used for the synthesis were reagent grade. The quadridentate Schiff base ligand H_2salpn was prepared by mixing salicylaldehyde and 1,2-diaminopropane in a 2:1 molar ratio in MeOH according to the literature [21, 22]. $[\text{Fe}(\text{salpn})\text{NO}_3]$ was prepared by mixing $\text{Fe}(\text{NO}_3)_3 \cdot 9\text{H}_2\text{O}$, H_2salpn and $\text{LiOH} \cdot \text{H}_2\text{O}$ in a 1:1:1.5 molar ratio in MeOH according to the method reported previously [23].

$[\text{Fe}(\text{salpn})]_2[\text{Fe}(\text{CN})_5\text{NO}]$ (1)

Well-shaped black crystals of (1) were obtained by slow diffusion of a dark brown MeOH solution (15 cm^3) of $[\text{Fe}(\text{salpn})\text{NO}_3]$ (0.15 mmol) and an aqueous solution (15 cm^3) of $\text{Na}_2[\text{Fe}(\text{CN})_5\text{NO}] \cdot 2\text{H}_2\text{O}$ (0.15 mmol) through a U-tube containing silica gel at room temperature. The resulting crystals were collected, washed with H_2O and MeOH respectively, and dried in air. (Found: C, 52.2; H, 3.75; N, 16.1; Fe, 19. $\text{C}_{39}\text{H}_{32}\text{Fe}_3\text{N}_{10}\text{O}_5$ calcd.: C, 52.7; H, 3.6; N, 15.8; Fe, 18.9%). I.r. ν_{max} (cm^{-1}): 2161(s), 1925(vs), 1629(vs), 1596(m), 1548(m), 1468(w), 1446(m), 1395(w), 1322(w), 1293(vs), 1149(w), 900(m), 800(m), 768(s), 615(m).

$[\text{Fe}(\text{salpn})]_2[\text{Ni}(\text{CN})_4]$ (2)

The complex was prepared as black single crystals in a way similar to that of complex (1), except for the use of $\text{K}_2[\text{Ni}(\text{CN})_4] \cdot \text{H}_2\text{O}$ (0.15 mmol) instead of $\text{Na}_2[\text{Fe}(\text{CN})_5\text{NO}] \cdot 2\text{H}_2\text{O}$. (Found: C, 55.1; H, 3.6; N, 13.3; Fe, 13.5; Ni, 7.1. $\text{C}_{38}\text{H}_{32}\text{Fe}_2\text{N}_8\text{NiO}_4$ calcd.: C, 54.65; H, 3.9; N, 13.4; Fe, 13.4; Ni, 7.0%). I.r. ν_{max} (cm^{-1}): 2155(s), 2133(s), 1628(vs), 1596(s), 1544(s), 1469(m), 1445(s), 1394(m), 1326(m), 1298(s), 1199(m), 1148(m), 903(m), 802(m), 761(s), 615(m), 449(m).

Table 1. Crystallographic data for (1) and (2)

	(1)	(2)
Formula	$\text{C}_{39}\text{H}_{32}\text{Fe}_3\text{N}_{10}\text{O}_5$	$\text{C}_{38}\text{H}_{32}\text{Fe}_2\text{N}_8\text{NiO}_4$
Formula weight	888.30	835.13
Crystal system	Tetragonal	Tetragonal
Space group	P 4/ncc	P 4/ncc
a (Å)	14.3982 (1)	14.250 (2)
b (Å)	14.3982 (1)	14.250 (2)
c (Å)	18.3434 (1)	18.322 (4)
V (Å ³)	3802.74(4)	3720.8 (11)
Z	4	4
D_c (g cm^{-3})	1.552	1.491
μ (mm^{-1})	1.188	1.322
Crystal size (mm^3)	$0.40 \times 0.375 \times 0.20$	$0.40 \times 0.375 \times 0.20$
θ range ($^\circ$)	2.00–25.97	2.22–25.97
Reflections measured	3568	1357
Independent reflections	1841 ($R_{\text{int}} = 0.0969$)	1355 ($R_{\text{int}} = 0.0227$)
Final R indices	$R_1 = 0.0698$	$R_1 = 0.0571$
$[I > 2\sigma(I)]$	$wR_2 = 0.1474$	$wR_2 = 0.1543$
Goodness-of-fit	0.931	0.962

X-ray crystallography

Diffraction data were collected at 293(2) K on Enraf-Nonius CAD4 and Rigaku AFC5R diffractometers for (1) and (2), respectively, using graphite-monochromated MoK_α radiation ($\lambda = 0.71073$ Å) with the ω - 2θ scan mode. The unit cell parameters were obtained by a least-squares refinement of the setting angles of 25 reflections with $11.92^\circ < \theta < 13.90^\circ$ for (1), and of 20 reflections with $15.60^\circ < \theta < 19.62^\circ$ for (2). The structures were solved by direct methods and refined by full matrix least-squares techniques based on F^2 . All non-hydrogen atoms were refined anisotropically and the sites of hydrogen atoms were placed by the geometry. The unweighted and weighted agreement factors of the forms $R_1 = \Sigma||F_0| - |F_c||/\Sigma|F_0|$ and $wR_2 = [\Sigma[w(F_0^2 - F_c^2)^2]/\Sigma[w(F_0^2)^2]]^{1/2}$ were used. The weighting schemes are $w = 1/[\sigma^2(F_0^2) + (0.0805P)^2 + 0.0000P]$ (1) and $1/[\sigma^2(F_0^2) + (0.0976P)^2 + 0.0000P]$ (2), where $P = (F_0^2 + 2F_c^2)/3$. All computations were carried out using the SHELXTL programs. The crystallographic data are summarized in Table 1.

Results and discussion

Spectroscopic studies

Relevant i.r. spectral data for complexes (1) and (2) are given in the Experimental section. The formation of cyanide bridges in both complexes is evidenced by the $\nu(\text{C}\equiv\text{N})$ stretching bands in the 2000–2200 cm^{-1} region. Complex (1) shows a sharp band at 2161 cm^{-1} , which can be attributed to the intermetallic bridging $\nu(\text{C}\equiv\text{N})$, as observed for other cyano-bridged complexes containing nitroprusside. The result also suggests that nearly all cyanide groups in $[\text{Fe}(\text{CN})_5\text{NO}]^{2-}$ are involved in coordination. A very strong band at 1925 cm^{-1} for (1) is reasonably assigned to the NO stretching vibration,

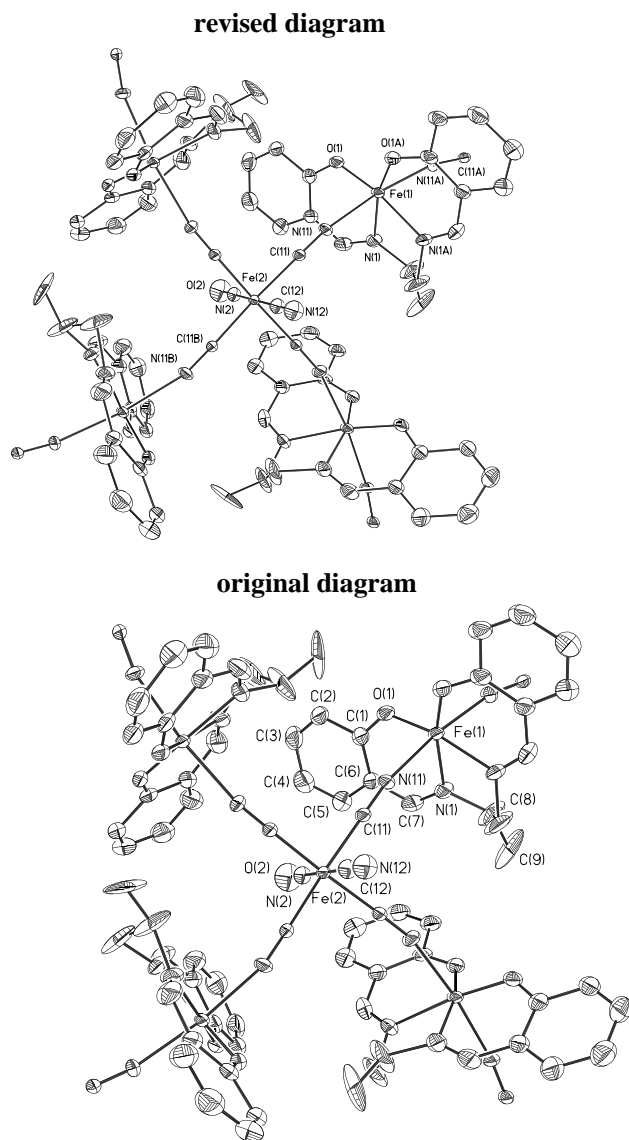


Fig. 1. ORTEP plot of complex (1).

thus implying that the Fe—N—O bond is linear [24]. Complex (2) shows two strong $\nu(\text{C}\equiv\text{N})$ bands at 2155 and 2133 cm^{-1} . The shift of $\nu(\text{C}\equiv\text{N})$ to higher wavenumbers relative to that of $\text{K}_2[\text{Ni}(\text{CN})_4]$ (2128 cm^{-1}) [25] suggests the formation of CN^- bridges. That $\nu(\text{C}\equiv\text{N})$ of bridging CN^- shifts to a higher frequency compared with that of terminal CN^- is largely attributed to kinematic coupling whereby the motion of bridging CN^- is constrained by the second metal center [26].

Crystal structures

An ORTEP diagram of $[\text{Fe}(\text{salpn})_2][\text{Fe}(\text{CN})_5\text{NO}]$ (1) with the atom numbering scheme is shown in Figure 1. The projection along the c -axis is given in Figure 2. The selected bond distances and angles are listed in Table 2. The molecular structure consists of one $[\text{Fe}^{\text{II}}(\text{CN})_5\text{NO}]^{2-}$ anion and two $[\text{Fe}^{\text{III}}(\text{salpn})]^+$ cations. Each $[\text{Fe}(\text{CN})_5\text{NO}]^{2-}$ anion coordinates with four $[\text{Fe}(\text{salpn})]^+$ cations *via* four equatorial $\text{C}\equiv\text{N}$ groups, whereas

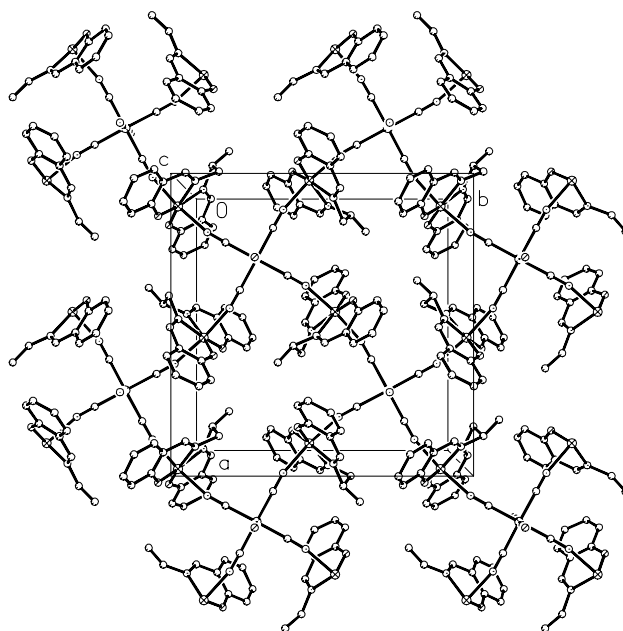


Fig. 2. Projection along the c -axis for complex (1), showing a 2D layer structure comprising of pillow-like octanuclear $[-\text{Fe}^{\text{II}}-\text{CN}-\text{Fe}^{\text{III}}-\text{NC}-]_4$ units.

Table 2. Selected bond lengths (Å) and angles ($^\circ$) for (1)

Bond lengths			
Fe(1)—O(1)	1.898(6)	Fe(1)—N(1)	2.111(7)
Fe(1)—N(11)	2.175(5)	Fe(2)—N(2)	1.64(1)
Fe(2)—C(12)	1.77(2)	Fe(2)—C(11)	1.930(6)
O(1)—C(1)	1.29(1)	O(2)—N(2)	1.16(2)
N(11)—C(11)	1.137(7)	N(12)—C(12)	1.19(2)
Bond angles			
O(1)#1—Fe(1)—O(1)	108.1(3)	O(1)—Fe(1)—N(1)#1	164.6(3)
O(1)—Fe(1)—N(1)	87.2(3)	N(1)#1—Fe(1)—N(1)	77.4(5)
O(1)#1—Fe(1)—N(11)	93.5(2)	O(1)—Fe(1)—N(11)	90.5(2)
N(1)#1—Fe(1)—N(11)	85.7(2)	N(1)—Fe(1)—N(11)	88.9(2)
N(11)—Fe(1)—N(11)#1	173.1(3)	N(11)—C(11)—Fe(2)	178.0(7)
C(12)—Fe(2)—C(11)	85.7(3)	N(2)—Fe(2)—C(11)	94.3(3)
C(11)—Fe(2)—C(11)#2	171.5(5)	C(11)—Fe(2)—C(11)#3	89.68(4)
C(1)—O(1)—Fe(1)	130.4(5)	C(7)—N(1)—Fe(1)	123.4(6)
C(8)—N(1)—Fe(1)	113.2(7)	C(11)—N(11)—Fe(1)	164.5(6)

Symmetry transformations used to generate equivalent atoms: (#1) $-y, -x, -z + 1/2$; (#2) $-x + 1/2, -y + 1/2, z$; (#3) $y, -x + 1/2, z$ and (#4) $-y + 1/2, x, z$.

each $[\text{Fe}(\text{salpn})]^+$ cation is linked to two $[\text{Fe}(\text{CN})_5\text{NO}]^{2-}$ ions in *trans* positions, which results in a 2D neutral layered structure consisting of pillow-like octanuclear $[-\text{Fe}^{\text{II}}-\text{CN}-\text{Fe}^{\text{III}}-\text{NC}-]_4$ units. The iron(III) ion in the $[\text{Fe}(\text{salpn})]^+$ unit assumes a slightly distorted octahedral coordination geometry in which the equatorial sites are occupied by N_2O_2 donor atoms of the quadridentate Schiff-base ligand salpn with $\text{Fe}^{\text{III}}-\text{N}$ and $\text{Fe}^{\text{III}}-\text{O}$ distances of 2.111(7) and 1.898(6) Å, respectively; and the axial positions are occupied by two nitrogen atoms from CN^- groups with $\text{Fe}^{\text{III}}-\text{N}$ distance of 2.175(5) Å and $\text{Fe}^{\text{III}}-\text{N}\equiv\text{C}$ angle of 164.5(6) $^\circ$. As usual, the $[\text{Fe}(\text{CN})_5\text{NO}]^{2-}$ fragment exhibits a distorted octahedral structure. The bond angle

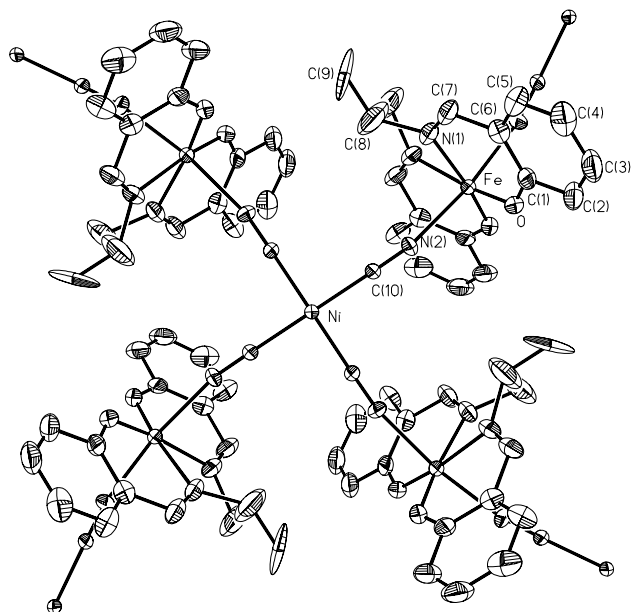


Fig. 3. ORTEP plot of complex (2).

of $\text{Fe}^{\text{II}}-\text{C}\equiv\text{N}$ is $178.0(7)^\circ$ for the bridging CN^- group. The terminal CN^- and NO ligands are co-linear as they both lie on the twofold axis that passes through iron(II). The $\text{Fe}^{\text{II}}-\text{CN}$ and $\text{C}\equiv\text{N}$ bond distances for bridging CN^- are $1.930(6)$ and $1.137(7)$ Å, respectively; whereas those for the terminal CN^- are $1.77(2)$ and $1.19(2)$ Å, which is accordance with that the antibonding electrons of CN^- are involved in coordination. The $\text{Fe}^{\text{II}}-\text{NO}$ and $\text{N}-\text{O}$ bond distances are $1.64(1)$ and $1.16(2)$ Å, respectively. All of these bond distances are comparable with those observed in other nitroprussides [27–33]. The $\text{C}(11)-\text{Fe}^{\text{II}}-\text{NO}$ angle (94.3°) is greater than 90° , whereas the $\text{C}(11)-\text{Fe}^{\text{II}}-\text{C}(12)$ angle (85.7°) is less than 90° . The greater electronegativity of the nitrosyl group with respect to the cyanide groups [34, 35] causes deformation away from the nitrosyl end of the octahedral geometry. As shown in Figure 2, the CN^- ligands bridge iron(II) and iron(III) centers to give a wave-like chain. The iron(II)··iron(III) and iron(III)··iron(III) separations within the chain are 5.188 and 10.182 Å, respectively. The nearest intralayer and interlayer iron(III)··iron(III) separations through space are 7.337 and 9.172 Å, respectively.

The labeled ORTEP plot of $[\text{Fe}(\text{salpn})]_2[\text{Ni}(\text{CN})_4]$ (2) is shown in Figure 3. Complex (2) is isomorphous with (1), and the selected bond distances and angles are listed in Table 3. The molecular structure consists of one $[\text{Ni}(\text{CN})_4]^{2-}$ anion and two $\text{Fe}(\text{salpn})^+$ cations. The anion and cation are linked by $\text{Ni}^{\text{II}}-\text{CN}-\text{Fe}^{\text{III}}$ assemblies to form a 2D neutral layered structure consisting of pillow-like octanuclear $[-\text{Ni}^{\text{II}}-\text{CN}-\text{Fe}^{\text{III}}-\text{NC}-]_4$ units. As usual, the $[\text{Ni}(\text{CN})_4]^{2-}$ moiety exhibits a square planar structure, in which the Ni(II) ion is located on a fourfold axis and coordinated by four CN^- ligands with Ni–C bond lengths of $1.867(6)$ Å and Ni–C≡N angles of $178.4(7)^\circ$. Each $[\text{Ni}(\text{CN})_4]^{2-}$ anion coordinates to four

Table 3. Selected bond lengths (Å) and angles ($^\circ$) for (2)

Bond lengths			
Ni–C(10)	1.867(6)	Fe–O	1.877(6)
Fe–N(1)	2.109(7)	Fe–N(2)	2.178(5)
N(2)–C(10)	1.128(8)	N(1)–C(7)	1.21(1)
Bond angles			
C(10)#2–Ni–C(10)	90	C(10)#3–Ni–C(10)	179.6(5)
O–Fe–O#4	106.4(4)	O–Fe–N(1)#4	165.8(3)
O–Fe–N(1)	87.8(3)	N(1)#4–Fe–N(1)	78.0(5)
O–Fe–N(2)#4	91.2(2)	N(1)–Fe–N(2)#4	86.5(3)
O–Fe–N(2)	93.2(2)	N(1)–Fe–N(2)	87.8(3)
N(2)#4–Fe–N(2)	172.6(3)	C(1)–O–Fe	130.2(5)
C(7)–N(1)–Fe	125.5(6)	C(8)–N(1)–Fe	112.1(7)
C(10)–N(2)–Fe	167.0(6)	N(2)–C(10)–Ni	178.4(7)

Symmetry transformations used to generate equivalent atoms: (#1) $y, -x + 1/2, z$; (#2) $-y + 1/2, x, z$; (#3) $-x + 1/2, -y + 1/2, z$ and (#4) $y - 1/2, x + 1/2, -z + 1/2$.

adjacent *trans*- $[\text{Fe}(\text{salpn})]^+$ cations through four cyano nitrogen atoms with a Fe–N distance of $2.178(5)$ Å and Fe–N≡C angle of $167.0(6)^\circ$. The coordination geometry of the iron(III) ion in the $[\text{Fe}(\text{salpn})]^+$ subunit is similar with that of (1). The $\text{Ni}^{\text{II}}\cdots\text{Fe}^{\text{III}}$ and $\text{Fe}^{\text{III}}\cdots\text{Fe}^{\text{III}}$ separations along the $-\text{Ni}^{\text{II}}-\text{C}\equiv\text{N}-\text{Fe}^{\text{III}}-$ linkage are 5.135 and 10.244 Å, respectively. The nearest intralayer and interlayer $\text{Fe}^{\text{III}}\cdots\text{Fe}^{\text{III}}$ separations through space are 7.244 and 9.345 Å, respectively.

It should be noted that in complexes (1) and (2), the $[\text{Fe}(\text{salpn})]^+$ fragment is bound by two equally strong π -bonding CN^- groups, which is different from those observed in the 2D $[\text{M}(\text{salen-substituted})]^+ / [\text{Fe}(\text{CN})_6]^{3-}$ adducts [19, 20, 36]. In addition, the interlayer distances of *ca.* 9.17 Å for (1) and 9.34 Å for (2) are much shorter than those of above adducts (13.10 – 16.57 Å), due to the lack of counteraction as spacer between two adjacent layers in present compounds. The salpn ligands in (1) and (2) have similar bonding parameters, which are comparable to those in relative complexes.

Magnetic properties

The cryomagnetic properties of complexes (1) and (2) are shown in Figures 4 and 5, respectively, in the forms of plots of χ_M and μ_{eff} versus T .

Complex (1)

The μ_{eff} per $\text{Fe}^{\text{III}}_2\text{Fe}^{\text{II}}$ unit at room temperature, $8.36 \mu_B$, is consistent with the spin-only value of $8.37 \mu_B$, which is expected for the magnetically dilute system consisting of two high spin iron(III) ions ($S = 5/2$) and one low spin iron(II) ion ($S = 0$), where the spin-only value was calculated by assuming $g_{\text{Fe}} = 2.00$. Lowering the temperature, the μ_{eff} value almost remains constant until 55 K, then decreases gradually in the 55 – 16 K range, and finally decreases sharply to $7.6 \mu_B$ at 5 K. The $1/\chi_M$ versus T plot obeys the Curie–Weiss law $\chi_M = C/(T-\theta)$ with a negative Weiss constant $\theta = -1.0$ K. These results indicate the existence of a weak antiferromagnetic interaction. As $[\text{Fe}(\text{CN})_5\text{NO}]^{2-}$ is diamagnetic, the

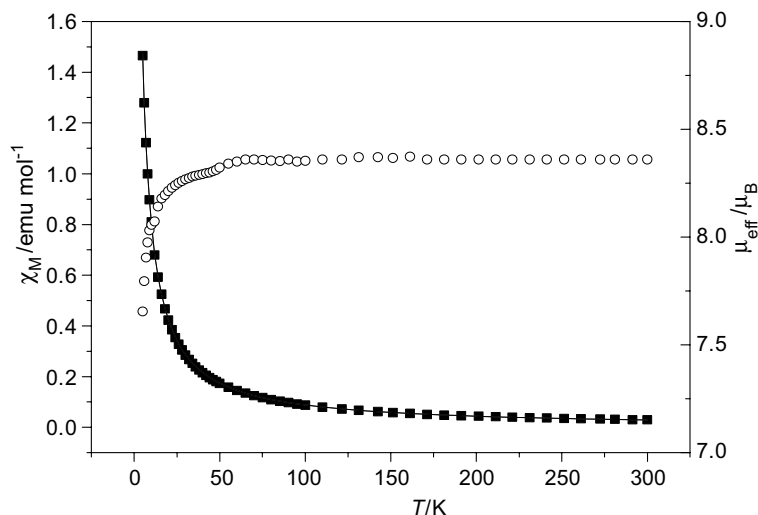


Fig. 4. The temperature-dependence of magnetic susceptibility χ_M (■ ■ ■) and the effective magnetic moment μ_{eff} (○ ○ ○). The solid line is the calculated curve discussed in the text.

exchange interaction between iron(II)–iron(III) through the cyanide bridging ligand is negligible. Based on the crystal structure, two exchange pathways are possible; one is the intralayer interaction between iron(III) ions through the diamagnetic $[\text{Fe}(\text{CN})_5\text{NO}]^{2-}$ units and the other is the interlayer interaction through space. Considering that the shortest iron(III)–iron(III) separation between the layers (9.172 Å) is longer than that within each layer (7.337 Å), the intralayer interaction is dominant and the interlayer interaction is negligible. Thus, the susceptibility can be expressed [37] by Equations (1)–(4).

$$\chi_t = \frac{2Ng^2\beta^2 A}{3kT} \frac{1}{B}, \quad (1)$$

where

$$A = 330 \exp(30J_t/kT) + 180 \exp(20J_t/kT) + 84 \exp(12J_t/kT) + 30 \exp(6J_t/kT) + 6 \exp(2J_t/kT),$$

$$B = 11 \exp(30J_t/kT) + 9 \exp(20J_t/kT) + 7 \exp(12J_t/kT) + 5 \exp(6J_t/kT) + 3 \exp(2J_t/kT) + 1.$$

$$\chi_t = \frac{Ng^2\beta^2}{3kT} S_t(S_t + 1), \quad (2)$$

$$\chi_{\text{chain}} = \frac{Ng^2\beta^2}{3kT} \frac{(1+u)}{(1-u)} \times S_t(S_t + 1), \quad (3)$$

where

$$u = \coth[J_c S_t(S_t + 1)/kT] - kT/J_c S_t(S_t + 1),$$

$$\chi_M = \frac{\chi_{\text{chain}}}{1 - \chi_{\text{chain}}(2zJ'/Ng^2\beta^2)}, \quad \text{where } z = 2, \quad (4)$$

where J_t , J_c and J' stand for the exchange integrals between two S_{Fe} ($S = 5/2$) spins within the $\text{Fe}_2^{\text{III}}\text{Fe}^{\text{II}}$ trimer, between the S_t effective spins of trimers and between the chains, respectively, and were treated as equivalent. The symbols N , g , β and k have their usual meanings. By allowing the g and J values to vary, we obtained the best fit to the experimental data with parameters $J_t = J_c = J' = -0.017 \text{ cm}^{-1}$, $g = 2.02$ and the disagreement factor $R = 7.9 \times 10^{-6}$ [$R = \sum(\chi_{\text{obs}} - \chi_{\text{calc}})^2 / \chi_{\text{obs}}^2$]. As shown in Figure 4, the fit may be considered to be good. The results ($J_t = J_c = J' < 0$) show the presence of a weak antiferromagnetic interaction between the nearest Fe^{III} ions within each sheet through the $-\text{NC}-\text{Fe}^{\text{II}}-\text{CN}-$ bridges.

Complex (2)

Complex (2) has similar magnetic behavior to that of (1). The μ_{eff} per $\text{Fe}_2^{\text{III}}\text{Ni}^{\text{II}}$ unit at room temperature, $8.0 \mu_B$, is slightly smaller than the spin-only value of $8.37 \mu_B$ expected for the magnetically dilute high spin iron(III) ions [$(S_{\text{Fe}}, S_{\text{Ni}}, S_{\text{Fe}}) = (5/2, 0, 5/2)$, where the spin-only value was calculated by assuming $g_{\text{Fe}} = 2.00$]. On lowering the temperature, the μ_{eff} value almost remains constant until 34 K, then decreases gradually in the 32–12 K range, and finally decreases sharply with further decreasing temperature to $7.3 \mu_B$ at 5 K. The magnetic susceptibility obeys the Curie–Weiss law with a negative Weiss constant $\theta = -1.1 \text{ K}$. These results indicate the existence of a weak antiferromagnetic interaction. As $[\text{Ni}(\text{CN})_4]^{2-}$ is diamagnetic, the exchange interaction between nickel(II)–iron(III) through the cyanide bridging ligand is negligible. However, the coupling between two adjacent iron(III) ions could occur through the $[\text{Ni}(\text{CN})_4]^{2-}$ group. Similar to complex (1), the susceptibility data for (2) can be approximated by Equations (1)–(4) with the best fit parameters $J_t = J_c = J' = -0.02 \text{ cm}^{-1}$, $g = 1.95$ and $R = 4.4 \times 10^{-6}$.

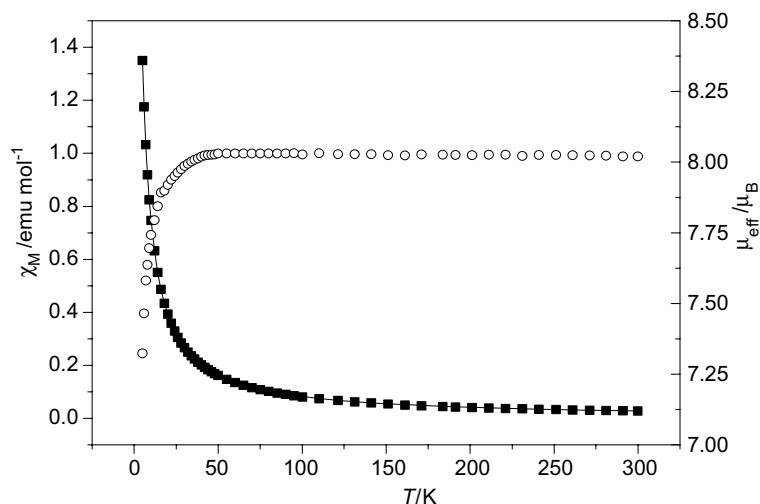


Fig. 5. The temperature-dependence of magnetic susceptibility χ_M (■ ■ ■) and the effective magnetic moment μ_{eff} (○ ○ ○) for (2). The solid line represents the fit discussed in the text.

(Figure 5). The results show the presence of weak intramolecular $\text{Fe}^{\text{III}} \cdots \text{Fe}^{\text{III}}$ antiferromagnetic interactions through the diamagnetic $-\text{NC}-\text{Ni}^{\text{II}}-\text{CN}-$ pathways.

It is observed that two paramagnetic centers usually give rise to weak antiferromagnetic interaction when bridged by the $[\text{Fe}(\text{CN})_5\text{NO}]^{2-}$ [27–30] or $[\text{Ni}(\text{CN})_4]^{2-}$ group [38–39], which can be rationalized by the long distance between paramagnetic centers. However, to our knowledge, the antiferromagnetic mechanisms for $[\text{Fe}(\text{CN})_5\text{NO}]^{2-}$ and $[\text{Ni}(\text{CN})_4]^{2-}$ are still unclear, and more works need to be done to clarify the exchange mechanism.

Supplementary data

Supplementary data are available from the Cambridge Crystallographic Data Center, 12 Union Road, Cambridge, CB2 1EZ, UK on request quoting the deposition numbers 193646 and 193647.

Acknowledgments

This work was supported by the Natural Science Foundation of the Bureau of Education of Jiangsu Province (No. 01KJB150010).

References

- M. Ohba and H. Okawa, *Coord. Chem. Rev.*, **198**, 313 (2000).
- M. Verdaguer, A. Bleuzen, V. Marvaud, J. Vaissermann, M. Seuleiman, C. Desplanches, A. Sculler, C. Train, R. Garde, G. Gelly, C. Lomenech, I. Rosenman, P. Veillet, C. Cartier and F. Villain, *Coord. Chem. Rev.*, **190–192**, 1023 (1999).
- W.P. Fehlhammer and M. Fritz, *Chem. Rev.*, **93**, 1243 (1993).
- K.R. Dunbar and R.A. Heintz, *Prog. Inorg. Chem.*, **45**, 283 (1997).
- A.H. Yuan, J.Z. Zou, B.L. Li, Z.G. Zha, C.Y. Duan, Y.J. Liu, Z. Xu and S. Keizer, *Chem. Commun.*, 1297 (2000).
- T. Mallah, S. Thiebaut, M. Verdaguer and P. Veillet, *Science*, **262**, 1554 (1993).
- W.R. Ently and G.S. Girolani, *Science*, **268**, 397 (1995).
- O. Kahn, *Nature*, **378**, 667 (1995).
- O. Sato, T. Iyoda, A. Fujishima and K. Hashimoto, *Science*, **272**, 704 (1996).
- S.M. Holmes and G.S. Girolami, *J. Am. Chem. Soc.*, **121**, 5593 (1999).
- E. Colacio, M. Ghazi, H. Stoeckli-Evans, F. Lloret, J.M. Moreno and C. Perez, *Inorg. Chem.*, **40**, 4876 (2001).
- H.Z. Kou, J.K. Tang, D.Z. Liao, S. Gao, P. Cheng, Z.H. Jiang, S.P. Yan, G.L. Wang, B. Chansou and J.P. Tuchagues, *Inorg. Chem.*, **40**, 4839 (2001).
- J. Larionova, M. Gross, M. Pilkington, H. Andres, H. Stoeckli-Evans, H.U. Gudel and S. Decurtins, *Angew. Chem. Int. Ed.*, **39**, 1605 (2000).
- M. Ohba, N. Usuki, N. Fukita and H. Okawa, *Angew. Chem. Int. Ed.*, **38**, 1795 (1999).
- Z.J. Zhong, H. Seino, Y. Mizobe, M. Hidai, A. Fujishima, S. Ohkoshi and K. Hashimoto, *J. Am. Chem. Soc.*, **122**, 2952 (2000).
- A. Marvilliers, S. Parsons, E. Riviere, J.P. Audiere, M. Kurmoo and T. Mallah, *Eur. J. Inorg. Chem.*, 1287 (2001).
- X.P. Shen, B.L. Li, J.Z. Zou, Z. Xu, Y.P. Yu and S.X. Liu, *Transition Met. Chem.*, **27**, 372 (2002).
- N. Re, E. Gallo, C. Floriani, H. Miyasaka and N. Matsumoto, *Inorg. Chem.*, **35**, 6004 (1996).
- H. Miyasaka, N. Matsumoto, H. Okawa, N. Re, E. Gallo and C. Floriani, *J. Am. Chem. Soc.*, **118**, 981 (1996).
- N. Re, R. Crescenzi, C. Floriani, H. Miyasaka and N. Matsumoto, *Inorg. Chem.*, **37**, 2717 (1998).
- P.J. McCarthy, R.J. Hovey, K. Ueno and A.E. Martell, *J. Am. Chem. Soc.*, **77**, 5820 (1955).
- P. Pfeifer, T. Hesse, H. Pfitzner, W. Scholl and H. Thielert, *J. Prakt. Chem.*, **149**, 217 (1937).
- N. Matsumoto, N. Takemoto, A. Ohyoshi and H. Okawa, *Bull. Chem. Soc. Jpn.*, **61**, 2984 (1988).
- P.N. Hawker and M.V. Twigg, in S.G. Wilkinson, R. Gillard and J.A. McCleverty (Eds), *Comprehensive Coordination Chemistry*, vol. 4, Pergamon, Oxford, 1989, p. 1187.
- K. Nakamoto, *Infrared and Raman Spectra of Inorganic and Coordination Compound*, 3rd edit., Wiley, New York, 1978, p. 259.
- S.Z. Zhan, D. Guo, X.Y. Zhang, C.X. Du, Y. Zhu and R.N. Yang, *Inorg. Chim. Acta*, **298**, 57 (2000).

27. Z.N. Chen, J.L. Wang, J. Qiu, F.M. Miao and W.X. Tang, *Inorg. Chem.*, **34**, 2255 (1995).
28. H.L. Shyu, H.H. Wei and Y. Wang, *Inorg. Chim. Acta*, **258**, 81 (1997).
29. H.Z. Kou, H.M. Wang, D.Z. Liao, P. Cheng, Z.H. Jiang, S.P. Yan, X.Y. Huang and G.L. Wang, *Aust. J. Chem.*, **51**, 661 (1998).
30. J.H. Zou, X.Y. Xu, Z. Xu, X.Z. You, X.Y. Huang, W.L. Zhang, X.P. Shen and Y.P. Yu, *J. Coord. Chem.*, **43**, 273 (1998).
31. N. Mondal, M.K. Saha, S. Mitra, V. Gramlich and M.S.E. Fallah, *Polyhedron*, **19**, 1935 (2000).
32. S. Zhan, X. Chen, A. Vij, D. Guo and Q. Meng, *Inorg. Chim. Acta*, **292**, 157 (1999).
33. J. Ribas, J.M. Julia, X. Aolans, M. Font-Altaba, A. Isalgue, X. Tejada, *Transition Met. Chem.*, **9**, 57 (1984).
34. J.E. Huheey, *J. Phys. Chem.*, **69**, 3284 (1965).
35. J.E. Huheey, *J. Phys. Chem.*, **70**, 2086 (1966).
36. H. Miyasaka, N. Matsumoto, N. Re, E. Gallo and C. Floriani, *Inorg. Chem.*, **36**, 670 (1997).
37. H.Z. Kou, W.M. Bu, D.Z. Liao, Z.H. Jiang, S.P. Yan, Y.G. Fan and G.L. Wang, *J. Chem. Soc., Dalton Trans.*, 4161 (1998).
38. Z. Smekal, I. Cisarova and J. Mrozinski, *Polyhedron*, **20**, 3301 (2001).
39. A.H. Yuan, X.P. Shen, Q.J. Wu, Z.X. Huang and Z. Xu, *J. Coord. Chem.*, **55**, 411 (2002).

TMCH 5688